- Technical Paper -

NUMERICAL SIMULATION OF HOLLOW PRECAST CONCRETE-FILLED STEEL TUBE PILES UNDER UNIAXIAL COMPRESSION

Clarissa JASINDA[*1], Naresh SUBEDI[*2], Taku OBARA[*3], and Susumu KONO[*4]

ABSTRACT

Three-dimensional finite-element analysis is conducted to investigate the detailed compressive behavior of hollow precast concrete-filled steel tube (hollow CFST) piles. From the calibration and verification of the model with experimental results, proper modeling parameters are discussed. Concrete damage plasticity model (CDPM) successfully captured the axial load (N)–average strain (ε_{avg}) curves of four hollow CFST specimens. The individual contributions of concrete and steel, and the development of confinement are also discussed to clarify the composite action.

Keywords: concrete-filled steel tube piles, hollow concrete core, high-strength concrete, compressive behavior, finite-element modeling

1. INTRODUCTION

Hollow precast concrete-filled steel tube (hereafter, hollow CFST) piles with circular section and high-strength concrete are common foundation members being used in Japan for low- or mid-rise buildings. These piles are used near the pile head where large shear force and deformation demands are expected during an earthquake. The diameter (D) ranges from 400 to 1500 mm, and diameter-to-steel thickness ratio (D/t_s) ranges from 50 to 100 [1]. Hollow CFST piles are manufactured in the factory by centrifugal concrete casting technique using high-strength concrete ($f_c' > 80$ MPa). These piles are expected to have high ductility because the concrete is restrained by the steel tube. Hollow CFST piles were originally developed to prevent the brittle damage of prestressed high-strength concrete (PHC) piles and prestressed reinforced concrete (PRC) piles. The steel tube prevents the explosive failure of these prestressed concrete piles, thus greatly improving the ductility.

From the survey conducted on 330 buildings with precast piles constructed between 2011 to 2017, 86% of them used hollow CFST piles [2]. Despite the high usage of this pile, there are only few guidelines to support the design of these piles. The AIJ 2008 Guidelines for CFT members [3] has been used to calculate the compressive capacity of hollow CFST piles. This guideline adopts the equation proposed by Sakino et al. [4] to compute the compressive capacity of cast-in-place CFST piles, in which they incorporated the concrete size-effect to reduce the compressive capacity of the concrete. This equation has been shown to work well for cast-in-place CFST members, but not for hollow CFST piles [5].

The author's research group has researched hollow CFST piles under flexural and constant axial loads [1]. It was found that this pile was very brittle under high axial loads. Eventually, the author's research group conducted two series of uniaxial compressive experiments [6,7] to understand the basic behavior of the pile. The results will be used to assess the mechanism of non-ductile post-peak flexural behavior of hollow CFST piles under high compressive load, and to propose a method to improve the ductility of hollow CFST piles. However, the mechanism and contribution of the concrete and steel tube could not be clearly observed in experiments and remains unclear. Several issues that need further investigation are the composite action (such as level of confinement and failure of concrete or steel), failure mechanisms, failure modes, and quantified contributions of each component.

In this study, the compressive behavior of hollow CFST piles is simulated by three-dimensional finite-element model to investigate the behavior which could not be directly observed during the experiment. Material models and modeling parameters appropriate for simulating the behavior of hollow CFST piles are identified considering the response and mechanisms observed in the experiment. Lastly, the detailed behavior of concrete and steel components are discussed to clarify the axial compression response of hollow CFST piles.

2. SPECIMEN DETAILS

Table 1 summarizes the details of the four hollow CFST pile specimens used for the finite-element analysis, and Fig. 1 shows the cross-section details of the piles. Material properties of concrete and steel tube are provided in Table 2. Details of the test setup and instrumentation are provided in reference [5]. Test

*1 Graduate Student, Dept. of Architecture and Building Eng., Tokyo Institute of Technology, JCI Student Member
*2 Post-doctoral Researcher, Institute of Innovative Research, Tokyo Institute of Technology
*3 Researcher, National Institute for Land and Infrastructure Management, JCI Member
*4 Professor, Institute of Innovative Research, Tokyo Institute of Technology, JCI Member

results are shown with the finite-element analysis results in Section 4.1.

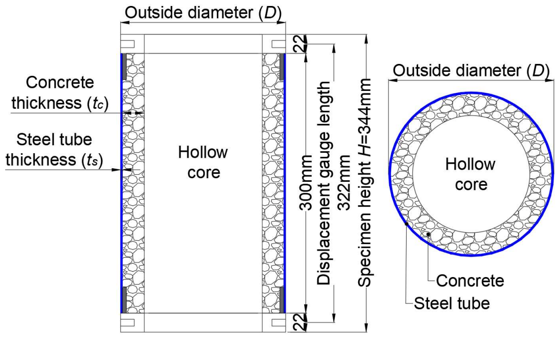

Fig. 1 Schematic of the hollow CFST pile specimens

Table 1 Details of tested specimens

Specimen Name	D [mm]	t_s [mm]	t_c [mm]	N_{exp} [kN]
SC25	190.8	2.3	25.8	1912
SC25s	190.6	5.3	26.1	2594
SC50	190.6	2.3	50.2	2864
SC50s	190.7	5.3	51.3	3542

*D, t_s and t_c are defined in Fig. 1. N_{exp} is the uniaxial compressive capacity obtained from experiment.

Table 2 Material test results

(a) Concrete

f_c' (MPa)	ε_c (μ)	E_c (GPa)	f_t (MPa)
120	2833	47.1	4.1

* The specimens were Ø100xH200 solid cylinders.
f_c': concrete compressive strength; ε_c: concrete compressive strain at peak strength; E_c: Young's modulus of concrete; f_t: concrete tensile strength.

(b) Steel tube

t_s (mm)	f_y (MPa)	ε_y (μ)	E_s (GPa)	f_{ts} (MPa)
2.3	273	3400	195	413
5.3	351	3632	215	431
7.0	349	3621	215	426

** The test coupons were obtained from the rolled tube in Fig. 1.
f_y: steel yield strength; ε_y: steel yield strain (based on 0.2% offset); E_s: Young's modulus of steel; f_{ts}: steel tensile strength.

3. FINITE-ELEMENT MODEL

3.1 Geometry and Element Details

A schematic of the finite-element model is shown in Figure 2. A commercial program, LS-DYNA, was used for the finite-element modeling of the hollow CFST specimens. Concrete was modeled using constant stress solid elements (ELFORM=1 in LS-DYNA). The steel tube was modeled using fully-integrated shell element modified for higher accuracy (ELFORM=-16), with three integration points, and a transverse shear stress factor of 5/6. The top and bottom plates are serving as the loading plate and seating plate, respectively, and were modeled using solid elements. These plates were

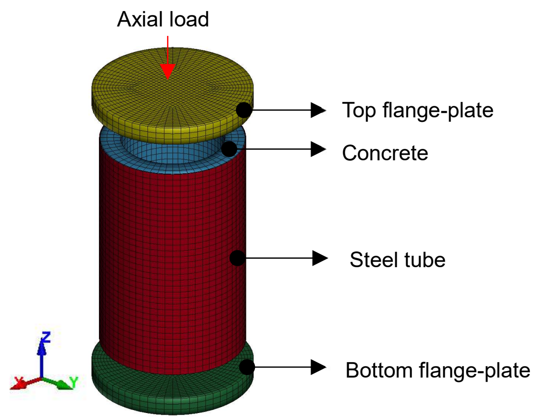

Fig. 2 Schematic of the numerical model

assigned a high stiffness to act as rigid components.

Static analyses were conducted using implicit solver of LS-DYNA. Contacts between concrete and steel tube, and concrete and top and bottom flange-plates were modeled using surface-to-surface mortar contact type with static friction coefficient (F_s) of 0.5. It is a segment-to-segment based contact, where the force transfer happens only when the neighboring segments are pushing and sliding against each other, but the contact will be lost when the segments are pulled (or separated) from each other. Mortar contact option is used for implicit analysis. For the contact between steel tube and flange-plates, tied constraint was used between the steel tube's shell edge and the flange-plates surfaces. This option simulates the welded connection between steel tube and flange-plates. The penetration of retained node to the constrained segment and vice-versa was prevented by specifying a very small penetration tolerance (PENMAX=1E-05 in LS-DYNA).

The bottommost part of bottom flange-plate was restrained in all degrees of freedom. Similar restraint was applied to the topmost part of top flange-plate, the difference being axial displacement (along the Z-axis) being allowed. Axial loading was applied as displacement along Z-axis for the top surface nodes of the top flange-plate.

3.2 Material Models

The material model used for the steel tube is bilinear material with strain hardening (material type 24 in LS-DYNA), as shown in Fig. 3. The input parameters were based on Table 2(b). Poisson's ratio of steel was taken as 0.3, and hardening stiffness, E_{TAN}, was computed as 0.5% of Young's modulus (E_s).

The concrete model used is concrete damage plastic model (material type 273 in LS-DYNA), developed by Grassl et al. [8], as shown in Fig. 4. This model is developed based on the combination of damage mechanics and plasticity to analyze the failure of concrete structures. For the compressive damage regime, exponential stress-inelastic strain law is used. A_{sf} is the ductility parameter during damage, set at the default value of 15. For high-strength concrete, parameter ε_{fc} was set to a small value of 0.00003. This small value represents the brittle damage in the post-peak region, where a sudden drop in capacity happens. The effect of

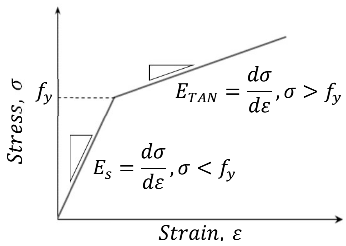

Fig. 3 Uniaxial stress-strain relationship of steel tube

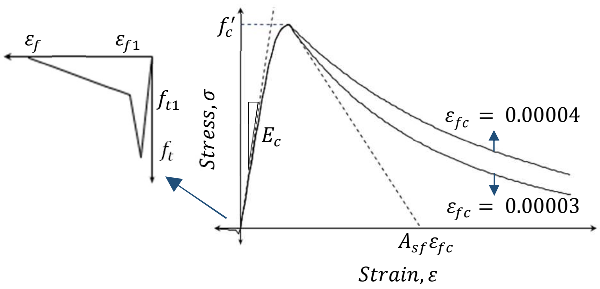

Fig. 4 Uniaxial stress-strain relationship of concrete

Table 3 Input parameters for Concrete Damage Plastic Model (CDPM) [8] in LS-DYNA

Parameter	Input	Description
ε_{fc}	0.00003	Parameter controlling compressive damage softening branch in the exponential damage formulation. Default = 0.0001
w_f	$4.444\ G_F/f_t$	Tensile displacement threshold value for linear tensile damage formulation, where: $G_F = 73{f_c'}^{0.18}$ $[N/m]$ (f_c' in MPa) is the fracture energy of concrete.
H_p	0.01	Hardening modulus. Value of 0.01 is recommended value for applications without strain rate effect.

parameter ε_{fc} on the concrete compressive response will be discussed in Section 4.1. Concrete size effect is not considered in the model, hence value of f_c' obtained from material model shown in Table 2(a) is directly used.

Tensile damage formulation of concrete is bilinear damage formulation as shown in Fig. 4. This relationship was obtained from the tensile stress–crack opening relationship using fracture energy (G_F) and element characteristic length (h). Inelastic strains ε_{f1} and ε_f are calculated as w_{f1}/h and w_f/h, respectively, where variable h is a mesh-dependent measure used to convert strains to displacements, and taken as finite element size. Variable w_f is specified in Table 3, and variable w_{f1} is taken as $0.15w_f$ (default value in LS-DYNA). The tensile strength of concrete (f_t) was calculated using Eq. (1) proposed by Arioglu et al. [9]. The f_t in from the material test results shown in Table 2(a) are not used.

$$f_t = 0.9[0.387(f_c')^{0.63}] \quad (1)$$

where f_t and f_c' are in MPa.

Parameters that were manually input are shown in Table 3. Other parameters that are not mentioned were set at default values.

4. RESULTS AND DISCUSSION

4.1 Model Calibration and Verification

In modeling hollow CFST, it is important to capture the peak capacity, the residual capacity, and the abrupt strength degradation. The parameter that is used to control these behaviors in the concrete model is the parameter ε_{fc}. Although ε_{fc} does not directly control the peak strength of concrete, with a high value of ε_{fc}, the concrete behaves in a ductile manner and, as a result, confining action might occur—increasing the peak capacity of the composite section. As an example, Fig. 5 shows the comparison of axial load (N)–average strain (ε_{avg}) relationship for specimen SC25 using different

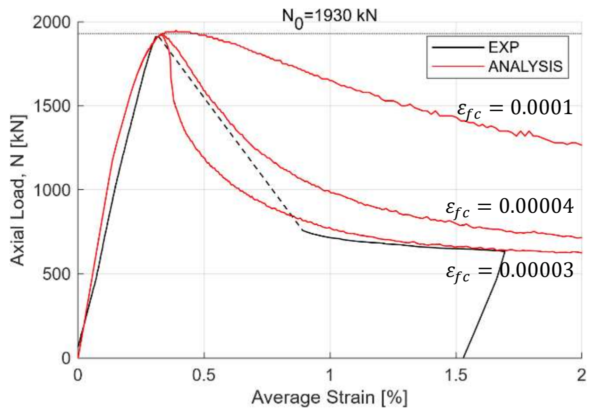

*The dashed line in experimental curve represents no data available due to the sudden capacity loss of specimen.

Fig. 5 Effect of parameter ε_{fc} on axial load (N)–average strain (ε_{avg}) response of specimen SC25

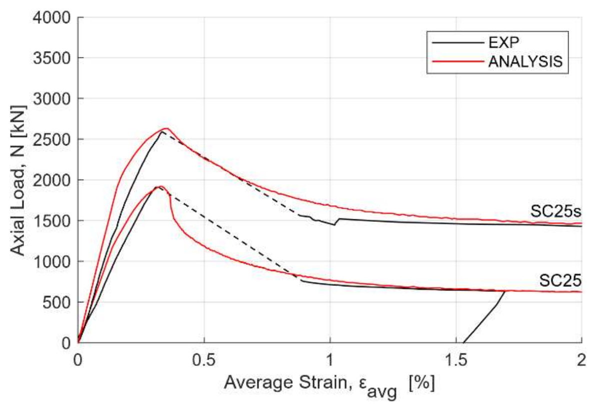

(a) Specimens SC25 and SC25s

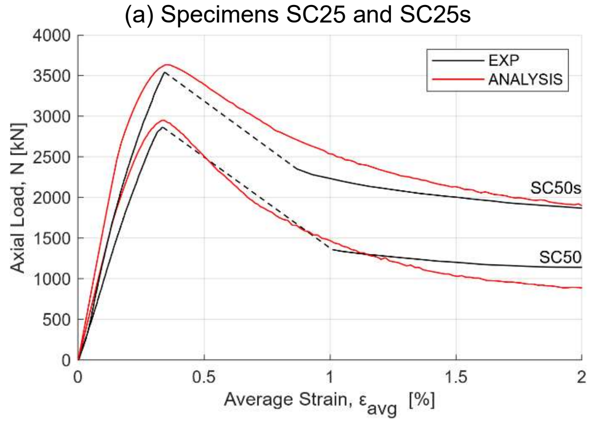

(b) Specimens SC50 and SC50s

Fig. 6 Comparison of axial load (N)–average strain (ε_{avg}) response from analysis and experiment

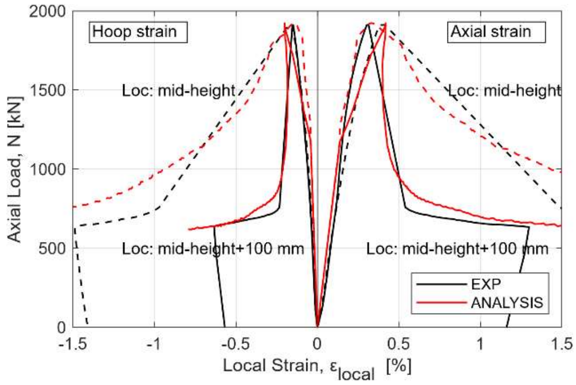

Fig. 7 Comparisons of strains in the steel tube of specimen SC25 measured at two locations (shown in Fig. 8)

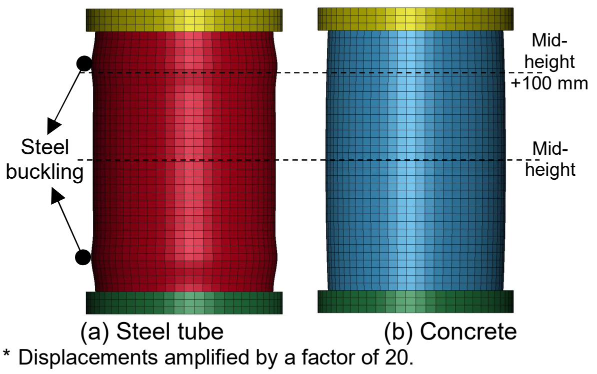

Fig. 8 Deformed shape of specimen No. 1 (SC25) at peak compressive capacity

values of parameter ε_{fc} (ε_{avg} is the ratio of axial displacement to the measurement length). When default value of 0.0001 was used, it can be seen in Fig. 5 that the strength degradation is very gradual which does not reflect the sudden strength degradation observed in the experiment. There is also a slight increase of capacity due to the confinement. Subedi et al. [10] recommended a range of ε_{fc} for cast-in-place CFSTs. This range is $0.00004 \leq \varepsilon_{fc} \leq 0.01$, where the smallest value was adopted from Vorel et al. [11] for plain concrete. When the smallest ε_{fc} for cast-in-place CFSTs was used for hollow CFST, it can be seen from Fig. 5 that the strength degradation is more gradual than the experimental results. For hollow CFSTs even the ε_{fc} value used for plain concrete does not seem appropriate because the high-strength concrete exhibits abrupt strength degradation and the hollow concrete section adds to the brittleness due to instability.

Since the hollow CFST with high-strength concrete shows more abrupt strength degradation, a smaller value of ε_{fc} was used. Figure 5 shows that using ε_{fc} of 0.00003 produced good agreement with the experimental results of specimen SC25. To validate the proposal of ε_{fc} =0.00003, the same model parameters were used to simulate the axial compression response of other three specimens (SC25s, SC50, and SC50s) listed in Table 1. Figure 6 shows the comparisons of the experimental and numerical results of the four specimens and Fig. 7 shows the local strains of the steel tube measured at two locations: mid-height and 100 mm above the mid-height level. Local strains in experiment were measured directly from the strain gauge. In finite-element model, the local strains were taken at the respective surface of the element. It can be observed from the figures that the simulated results are in good agreement with the experimental results, and thus the model captures the peak capacity and the post-peak behavior.

The ability of the model to accurately reproduce the global behavior of four specimens and to also accurately reproduce the local steel strains in two regions gives confidence that the model can be used to examine the behavior not observed in the experiment. For example, Fig. 8 shows steel buckling at approximately ¼ and ¾ of the height. In the experiment, steel buckling at the peak compressive load was not visually observed. In finite-element simulation, however, the steel buckling can be clearly seen when the displacement is amplified by 20 times.

4.2 Detailed Response from Finite-element Analysis

Given the good results of the finite-element model, it will be used to investigate the individual contributions of the steel and concrete in the hollow CFST pile.

4.2.1 Change in Behavior Due to Composite Action

It is well-known that composite members show different response when compared to the behavior of each separate individual component (i.e., hollow concrete, hollow steel tube). In this subsection, the individual contribution of concrete and steel in the hollow CFST is compared with the behavior of individual components acting separately.

Figure 9 shows the comparison of analysis results for: 1) plain concrete cylinder, 2) hollow concrete core-only model of SC25, 3) hollow steel tube-only model of SC25; and 4) SC25 specimen with individual contributions of concrete and steel tube. Same material properties were used for all models. The lines in Fig. 9 are split into Fig. 10(a) and (b), and Y-axes are changed into axial stresses (σ) for easier comparison.

Figure 10(a) shows detailed comparisons of steel tube axial stress (σ)–average strain (ε_{avg}) curves. Comparing hollow steel tube-only model of SC25 and the contribution of the steel tube in SC25 CFST model, it can be seen that the post-peak response of the steel does not have the strength degradation of the steel-only model, likely because the steel local buckling in the mid-height region is prevented by the presence of concrete. In the hollow steel tube model, the capacity gradually decreases due to steel buckling. For the steel tube contribution extracted from the hollow CFST model, the steel tube loses some strength immediately after the peak, which is seen from the sudden drop of the capacity, and regains the capacity and does not show any capacity decrease even at later stage of loading. The residual capacity ratio from the experiment (N_{res}/N_{exp}, where N_{res} is the residual capacity) is 34% at an average strain of 1.5%. At the same average strain, the residual capacity ratio of hollow steel tube model is 10%, while that for the steel tube from SC25 model is 20%. The enhance-

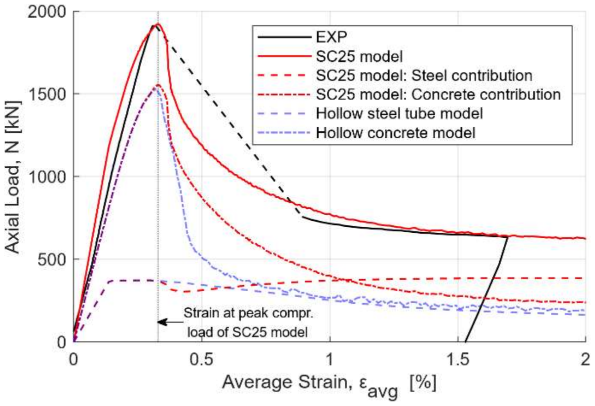

Fig. 9 Axial load (N)–average strain (ε_{avg}) of specimen SC25 model with hollow steel tube and hollow concrete models

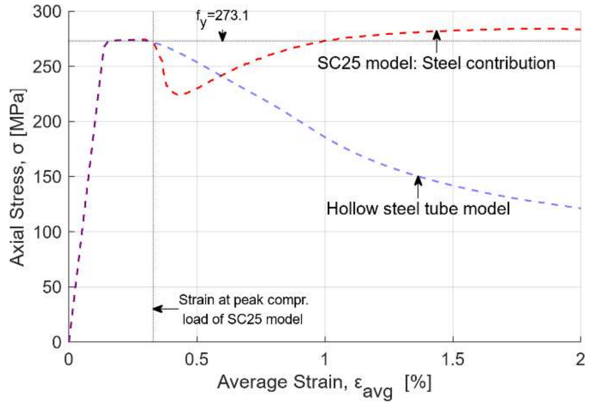

(a) Steel tube

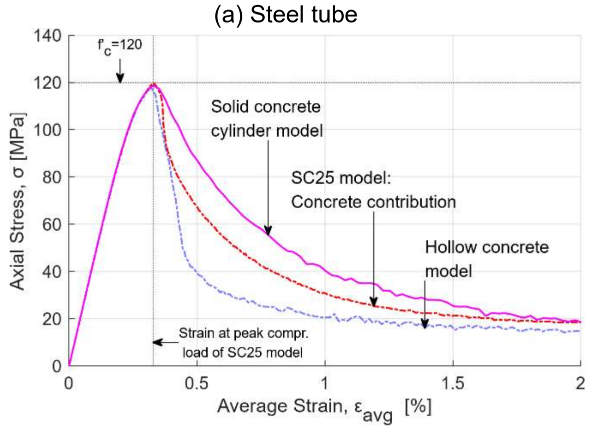

(b) Concrete

Fig. 10 Comparisons of axial stress (σ)–average strain (ε_{avg}) of specimen SC25 model with separate concrete and steel models

ment is double for this case.

Comparing the plain solid concrete cylinder model and hollow concrete-only model of SC25 in Fig. 10(b), it is observed that the hollow concrete is more brittle as shown by the sudden drop in capacity and smaller residual capacity. The residual capacity of the hollow concrete is lower than plain concrete. This difference in behavior is expected because the hollow concrete is more unstable and brittle than the solid plain concrete cylinder.

When comparing concrete contribution from the SC25 model with the hollow concrete model, both models show identical behavior up to the peak. The initial post-peak drops are also very similar. However, the concrete in the hollow CFST retained more residual capacity (14%) than the plain hollow concrete (11%). Hence, it can be inferred that the presence of the steel tube helps in retaining the residual capacity of concrete because it slightly improves the residual capacity of the concrete. However, the improvement of concrete residual strength due to composite action is less than the improvement of the steel tube.

4.2.2 Confinement Effect

Although previous researches suggested that there is confinement action in hollow CFSTs [12,13,14], the presence of confinement in hollow CFSTs with high-strength concrete is questionable [5]. Therefore, we used the finite-element model to investigate the presence of confinement by observing the hoop stress in the steel tube.

The stresses in the steel tube at mid-height level obtained from the model are plotted in Fig. 11. The average axial stress of concrete is also shown in the figure. In addition, strain corresponding to the peak axial load is also marked in the figure. In Fig. 11(a), it can be seen that very small hoop stress is developed in the steel tube (with D/t_s=83) before the peak axial capacity is reached. The hoop stress in the steel tube is more prominent for SC25s, which has thicker steel tube (Fig. 11(b)) of t_s=5.3 mm (D/t_s=36). At the peak axial capacity, the average axial stress in concrete of SC25s (Fig. 11(b)) also has slight increase (≈3%) from f'_c, whereas in specimen SC25 (Fig. 11 (a)) with t_s=2.3 mm (D/t_s=83), there is no increase in concrete capacity on average. Although not shown in this paper, similar

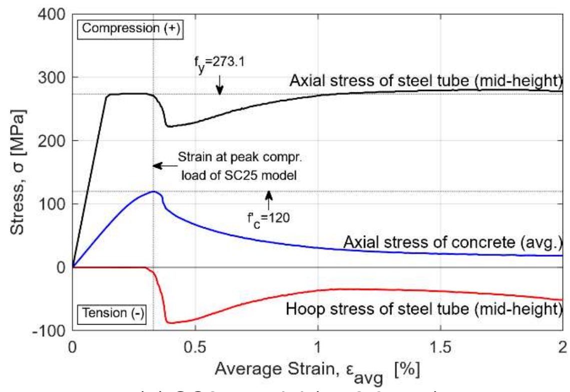

(a) SC25 model (t_s=2.3 mm)

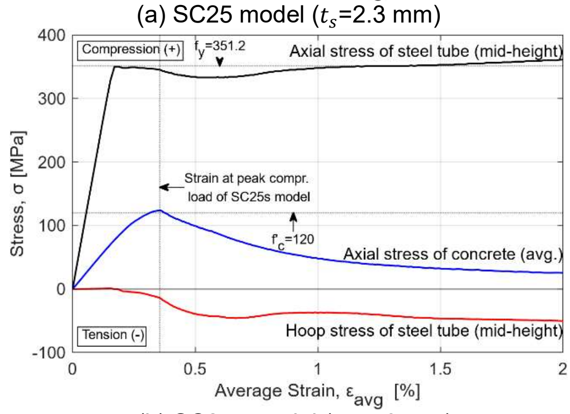

(b) SC25s model (t_s=5.3 mm)

Fig. 11 Axial and hoop stresses of steel and concrete from analysis results are observed for specimens SC50 and SC50s. From these observations, it can be concluded that there is only slight confinement in hollow CFSTs, if any, and the confinement slightly improves when steel tube is thicker. For smaller D/t_s, the steel tube in the mid-height region develops local buckling much slower, therefore the lateral expansion of concrete catches up with the steel expansion, and hoop stress is developed at an earlier stage.

In addition, if we compare the axial stress in the steel tube for the two specimens, the specimen with thicker steel tube (SC25s) shows a slight decrease from its yield strength, f_y, at the peak axial load. It is also observed that the strength degradation resulting from local buckling of steel tube is prevented when the steel is thicker.

5. CONCLUSIONS

Three-dimension finite-element model of hollow CFSTs with the concrete damage plasticity model (CDPM) developed by Grassl et al. [8] successfully simulated the axial load (N)–average strain (ε_{avg}) relationships of four specimens under monotonic compressive loading. The following conclusions are drawn from this study.

(1) In CDPM model, parameter ε_{fc} is used to control the concrete brittleness in the post-peak region, where value of 0.00003 well-captured the compressive behavior of the four hollow CFST specimens. This value is smaller than the minimum value used for plain solid concrete (ε_{fc}=0.00004) which indicates that even with the presence of steel tube, hollow concrete in CFST sections is more unstable and brittle compared to plain concrete.

(2) CFST sections showed different behaviors compared to hollow concrete and hollow steel tube. In the hollow CFST section, the capacity loss of steel tube is prevented and the concrete retains more residual capacity.

(3) The finite-element analysis showed that the steel tube gives the most contribution to the residual capacity of hollow CFST. Therefore, it is recommended to increase steel tube thickness (t_s) to increase the residual capacity of the hollow CFST.

(4) For high-strength concrete in a hollow CFST, confinement effect was found to be very small when steel tube is thin (t_s =2.3 mm, D/t_s =83). Confinement effect slightly improves when steel tube becomes thicker (t_s =5.3 mm, D/t_s =36), however, is only slightly noticeable (≈3% of f_c'). Confinement effect can be neglected when calculating the compressive capacities of hollow CFST specimens.

ACKNOWLEDGEMENT

The first author gratefully acknowledges the Ministry of Education, Culture, Sports, Science, and Technology (MEXT), Japan for funding her graduate study at Tokyo Institute of Technology. The authors thank COPITA for their financial support and valuable opinions.

REFERENCES

[1] Thusoo S et al., "Design models for steel encased high-strength precast concrete piles under axial-flexural loads," *Eng. Struct.* 228 (2021): 111465

[2] Kaneko O, "Surveys on actual applicable conditions of concrete pile foundations for seismic design against severe earthquakes," *AIJ J. Technol. Des.* (2017), Vol. 23, No. 53: 87–92. [In Japanese].

[3] Architectural Institute of Japan. *Recommendations for Design and Construction of Concrete Filled Steel Tubular Structures (2nd edition)*. AIJ: Tokyo, Japan, 2008. [in Japanese].

[4] Sakino K, Nakahara H, Morino S, Nishiyama I, "Behavior of centrally loaded concrete-filled steel-tube short columns," *ASCE Journal of Structural Engineering* 130(2) (2004): 180-188.

[5] Jasinda C et al., "Uniaxial compressive behavior of high-strength circular hollow centrifugal concrete-filled steel tubular piles," *Proceedings of the Japan Concrete Institute*, 44, 2, 571-576, JCI, 2022.

[6] Furukawa K, Jasinda C, et al., "Uniaxial compression test on precast and cast-in-situ CFST piles," *Summary of Technical Papers of Annual Meeting*, *Vol. IV*, *603-606*, AIJ, 2021. [in Japanese].

[7] Jasinda C et al., "Uniaxial compressive behavior of hollow circular high-strength precast concrete-filled steel tubular piles (part 1-2)," *Summary of Technical Papers of Annual Meeting*, *Vol. IV*, *485-488*, AIJ, 2022. [in Japanese].

[8] Grassl P, Xenos D, Nyström U, Rempling R, Gylltoft K, "CDPM2: A damage-plasticity approach to modelling the failure of concrete," *Int. J. of Solids Struct.* (2013), Vol. 50, 24: 3805-3816.

[9] Arioglu N, Girgin ZC, and Arioglu E, "Evaluation of ratio between splitting tensile strength and compressive strength for concretes up to 120 MPa and its application in strength criterion," *ACI Materials Journal* 103(1) (2006): 18-24.

[10] Subedi N et al., "Noncompact and slender concrete-filled steel tubes under axial compression: Finite-element modeling and evaluation of stress-strain models for fiber-based analysis," *Journal of Cons. Steel Research* 196 (2022): 107353.

[11] Vorel J, Marcon M, Cusatis G, Caner F, Di Luzio G, Wan-Wendner R, "A comparison of the state of the art models for constitutive modelling of concrete," *Comput. Struct.* 244 (2021): 106426.

[12] Miyaki S, Matsui C, Tsuda K, Hatato T, Imamura T, "Evaluation formula of compressive strength of centrifugal concrete filled steel circular tubular columns using supper high strength concrete," *AIJ J. Struct. Constr. Eng.* (1996), Vol. 61, No. 482: 151-160. [in Japanese].

[13] Yu M, Zha XQ, Ye JQ, She CY, "A unified formulation for hollow and solid concrete-filled steel tube columns under axial compression," *Eng. Struct.* 32(4) (2010): 1046–1053

[14] Zhao YG, Yan XF, and Lin S, "Compressive strength of axially loaded circular hollow centrifugal concrete-filled steel tubular short columns," *Eng. Struct.* 201 (2019): 109828.